

# The volumetrically averaged dose gradient at the target volume's boundary and within the target volume

Markus Wösle\*

Klinik für Strahlentherapie und Radioonkologie, Städtisches Klinikum Dessau, Dessau-Roßlau, Germany.

## ABSTRACT

ICRU Report 91 recommends two dose gradient metrics for reporting in stereotactic radiotherapy. All of the common gradient indices are one-dimensional although clinical dose gradient problems are at least two-dimensional. Moreover, a loss of accuracy is inherent in two-dimensional dose gradient measures like the superficially averaged dose gradient (*SADG*) due to the linearization in the third dimension. To close this information gap, the author developed a three-dimensional dose gradient measure called the volumetrically averaged dose gradient (*VADG*). The correlations between eleven one-dimensional and three two-dimensional dose gradient measures on the *VADG* were investigated for the linac-based stereotactic radiosurgery of 13 brain metastases. Dose gradient distributions were illustrated by vector fields, dose gradient-frequency histograms, and dose-dependent dose gradient functions. From all of the one-dimensional dose gradient indices, the approximated *SADG*\* showed the strongest correlation on the *VADG*. The relative errors were in a range of -18.9 to 3.2% and Pearson's correlation coefficients were  $r \geq 0.997$ . The *SADG* showed the strongest correlation on the *VADG* of all of the two-dimensional dose gradient measures with the relative errors in a range of -14.8 to -9.6% and  $r \geq 0.999$ . Three-dimensional dose gradient measures like the *VADG* best describe dose gradient distributions for lesions that are located in non-homogeneous normal tissue. The quality of each dose gradient measure concerning the description

of anisotropic dose gradient distributions is now verifiable. The algorithm for determining the *VADG* should be implemented in treatment planning and patient plan verification systems to utilize the formalism for all users.

**KEYWORDS:** anisotropic dose gradient distribution, multi-dimensional dose gradient measure, superficially averaged dose gradient, superficially averaged radius difference, volumetrically averaged dose gradient.

## 1. INTRODUCTION

Quality criteria in radiotherapy to specify the dose distribution within the target volume and at its boundary are the dose homogeneity, dose conformity, and irradiated volume. ICRU Report 62 and ICRU Report 83 recommend reporting the values of these parameters [1, 2]. Particularly in stereotactic radiotherapy and radiosurgery, clinical complications primarily occur due to the dose fall-off in a region between the surfaces of the prescribed isodose and another isodose defining the irradiated volume with an organ-specific tolerance dose level. Consequently, good dose conformity and steep dose gradients are necessary and sufficient conditions for sparing doses in healthy tissue.

The dose fall-off at the target volume's boundary can be characterized by different dose gradient measures or indices. ICRU Report 91 recommends reporting one of two simple dose gradient indices [3]: the dose gradient index (*GI*) of Paddick *et al.* [4] or the volume of normal tissue irradiated with at least the dose  $D$ ,  $V_D$ , for instance,  $D = 12$  Gy for brain tissue [5, 6]. The aim is to better associate the

---

\*Corresponding author  
markus.woesle@klinikum-dessau.de

treatment complications with the values of dose gradient indices *via* rigorous and uniform reporting of these parameters [3].

Since 2000, several dose gradient indices have been defined that are all one-dimensional and based on

- single volumes of the irradiated tissue [5, 6],
- volume ratios of the isodoses of interest [4, 7, 8],
- ratios of real and ideal volumes of the irradiated tissue [9],
- radius differences between the isodoses of interest [10-12],
- dose difference quotients [13], or
- combinations of a dose gradient index with different indices, for example, for dose conformity [14, 15].

The definitions and explanations of the aforementioned dose gradient indices were concisely presented in [16]. Additionally, the shortcomings of the one-dimensional dose gradient indices in [4-12, 14, 15] were specified and discussed in [16].

Furthermore, ICRU Report 91 and other publications stated additional deficiencies of selected dose gradient indices [4-8, 15]:

- The reporting of the *GI* per target volume is not realistic for treatment plans containing multiple targets with one common surface of the distal isodose of interest [3]. In addition, the *GI* yields false superior values in cases of prescribed isodoses that exaggerate the target volume's coverage [8].
- The metric  $V_D$  is not suited for comparing quality between treatment plans for varying target volume sizes treated with different doses [3]. Moreover,  $V_{12\text{ Gy}}(\text{Brain})$  underestimates physical dose gradients [16].
- The *GI*, the dose gradient (*DG*), and the modified dose gradient index (*mGI*) overvalue physical dose gradients [16].
- Indifferent values of these dose gradient indices can occur even though the physical dose gradient considerably varies [16].
- The values of the volume ratio (*VR*) are dependent on the prescription isodose [4].

All deficiencies taken together entail that the aforementioned aim of ICRU Report 91 is unattainable. In particular, the use of the *GI*, *DG*, and *mGI* regularly vexes medical physicists and

radiation oncologists whenever multiple targets of different sizes must be irradiated: Why is the dose gradient of the larger target volume better than that of the smaller one, and vice versa?

In 2019, the first two-dimensional dose gradient measures were published to get rid of all of the aforementioned intrinsic shortcomings of one-dimensional dose gradient indices. They are called the superficially averaged dose gradient (*SADG*) and the superficially averaged radius difference ( $\overline{\Delta r_{\Delta D}}$ ) between the isodoses of interest. Its definitions are summarized in Appendices A.1 and A.2. Both quantities are globally defined for the nonspecific normal tissue as well as locally for all of the organs at risk. A mathematical approach has been developed for treatment plans with multiple targets if one isodose of interest encompasses more than one target volume [16]. The two-dimensional dose gradient measures linearize the dose gradients in the radial direction, which results in a loss of accuracy – one intrinsic shortcoming of this class of dose gradient measures.

All of the gradient measures aid assessing treatment plans concerning clinical suitability and predicting the degree of severity of radiogenic side effects in critical structures. In this context, an adequate quality of the description of anisotropic dose gradient problems is one necessary condition for the suitability of a dose gradient measure for predicting normal tissue complication probabilities.

To obtain clear and exact predications about highly anisotropic dose gradient distributions and local dose gradients, a new three-dimensional dose gradient measure without any accuracy loss is defined herein: the volumetrically averaged dose gradient (*VADG*).

The present article will assess the one- and two-dimensional dose gradient measures that optimally quantify the mean value of the physical dose gradients. All of the dose gradient measures were applied in one linac-based irradiation series for the stereotactic radiosurgery of 13 globular brain metastases. The *VADG* was globally calculated for the nonspecific normal tissue. The possible correlations between the *VADG* and the other dose gradient measures were investigated. Graphical results of three-dimensional dose gradient distributions are also presented.

## 2. MATERIALS AND METHODS

### 2.1. Definitions of common dose gradient indices

The new three-dimensional dose gradient measure *VADG* yields reference values to investigate the quality of all of the common one- and two-dimensional dose gradient measures. For a better traceability of the findings, the definitions of the common one-dimensional dose gradient indices are summarized in Appendix A.1 of [16]. For the definitions of the two-dimensional dose gradient measures, see Appendices A.1 and A.2 below.

### 2.2. Formulations of anisotropic dose gradient problems

The spatial distribution of the dose gradients at the boundary of a target volume is written in spherical coordinates because the dose gradients in the radial direction are of interest. For explanation, the radial dose gradient vectors are approximately perpendicular to the surfaces of the treated and irradiated volumes and enable the description of the spatial dose gradient distributions. The system of spherical coordinates  $K_S = \{O, r, \varphi, \vartheta\}$  is defined by the origin  $O$  in the geometrical mass centre of the target volume and the three curvilinear coordinates: radius  $r$ , azimuth  $\varphi$ , and polar distance angle  $\vartheta$ .

From a mathematical perspective, two different anisotropic formulations with spherical coordinates are conceivable:

- The dose gradients are two-dimensional in  $\varphi$  and  $\vartheta$  and will be linearized along  $r$  by the difference quotients. This is the rationale for the already published dose gradient measure called *SADG* [16].
- The dose gradients are three-dimensional in all spherical coordinates and will be described by the vector field of dose gradients. This is the rationale for the new dose gradient measure *VADG* (see Subsection 2.2.1).

The system of Cartesian coordinates  $K_C = \{O, x, y, z\}$  can also be used to describe multi-dimensional dose gradient problems. The anatomical directions will be right to left ( $x$ ), anterior to posterior ( $y$ ), and inferior to superior ( $z$ ) in the patient position head first, supine if DICOM coordinates are used.

#### 2.2.1. Volumetrically averaged dose gradient

The following formulation is based on the discrete dose matrix  $D = D(x, y, z) \in \mathbb{R}$ . It is a scalar field in the coordinate system  $K_C$ . The related vector field of dose gradients  $\nabla \cdot D(x, y, z) \in \mathbb{R}^3$  can be transformed into the scalar field of dose gradient magnitudes  $\|\nabla \cdot D(x, y, z)\| \in \mathbb{R}$  by performing the Euclidean norm.

In general, the resultant dose gradient vectors do not appear in the radial direction. Before the definition of the three-dimensional dose gradient measure, the radial projection

$$\|\nabla \cdot D(x, y, z)\|_{proj} = \|\nabla \cdot D(x, y, z)\| \cdot \cos(\varphi_{\nabla} - \varphi) \cdot \cos(\vartheta_{\nabla} - \vartheta) \in \mathbb{R}_0^+ \quad (1)$$

must be performed.  $\varphi$  and  $\vartheta$  are the azimuths and polar distance angles of the radius vectors  $\mathbf{r} = (x, y, z)^T$  written in spherical coordinates. Furthermore,  $\varphi_{\nabla}$  and  $\vartheta_{\nabla}$  are the azimuths and polar distance angles of the local dose gradients  $\nabla \cdot D(x, y, z)$  transformed into the spherical coordinate system  $K_S$ .

The integral mean value of the scalar dose gradient function  $\|\nabla \cdot D(x, y, z)\|_{proj}$  for the nonspecific normal tissue between the isodose levels  $D_1$  and  $D_2$  is the result of applying the generalised first mean value theorem for integration to volume integrals:

$$VADG_{proj}(NT)|_{D_2}^{D_1} = -\frac{1}{V_{\Delta D}(NT)} \cdot \iiint_{[V_{\Delta D}(NT)]} \|\nabla \cdot D(x, y, z)\|_{proj} \cdot dx \cdot dy \cdot dz \in \mathbb{R}^-, \quad (2)$$

where

$$V_{\Delta D}(NT) = V(D_1, D_2) = \{\mathbf{r} \mid D_1 \geq D(\mathbf{r}) \geq D_2\} \in \mathbb{R}^+, \quad \mathbf{r} = (x, y, z)^T \quad (3)$$

is the volume range of integration. The negative sign in Eq. (2) indicates the dose fall-off beginning at the boundary of the target volume towards the normal tissue.

The  $VADG_{min}(NT)|_{D_2}^{D_1}$  calculated with the minimal – steepest – dose gradients is determined according to Eq. (2) with the integrand  $\|\nabla \cdot D(x, y, z)\|$ . The impact of the dose gradient direction on the values

of the three-dimensional dose gradient measure can be investigated by comparisons between the  $VADG_{proj}$  and  $VADG_{min}$ .

The calculation of the organ-specific dose gradient measure  $VADG(OAR_i)|_{D_2}^{D_1}$  requires two substitutes in Eq. (2): the integration interval and the volume in the left multiplication factor. The integration interval and volume for an arbitrary organ at risk  $OAR_i$  are

$$V_{\Delta D}(OAR_i) = \{\mathbf{r} \mid D_1 \geq D(\mathbf{r}) \geq D_2 \wedge t \cdot \mathbf{r} \in V_{OAR_i}\} \in \mathbb{R}^+, \quad \mathbf{r} = (x, y, z)^T, \quad t \in \mathbb{R}^+ \quad (4)$$

and must be applied with the volume integral of the function in Eq. (1).  $t$  is a positive real number, and  $V_{OAR_i}$  is the volume of  $OAR_i$ .

### 2.2.2. Statistics and histograms of dose gradient distributions

The mean value of the  $VADG$  is not the sole result because all of the local function values of the integrands

$$\|\nabla \cdot D(x, y, z)\|, \|\nabla \cdot D(x, y, z)\|_{proj} = f(x, y, z) \in \mathbb{R}_0^+ \quad (5)$$

in Eq. (1), which quantify dose gradient distributions, are known during the integration process. Additionally, the values of further statistical measures of location and dispersion are available: median, modal value, range, standard deviation, and percentiles.

The differential and cumulative dose gradient-frequency histograms, where the frequency is a function of the dose gradient, are defined for a compact visual presentation of the statistical results for the nonspecific normal tissue and organs at risk. The values of two different absolute or relative quantities can be applied along the ordinate: frequency or volume.

### 2.2.3. Dose-dependent dose gradient measure

The algorithm for calculating the  $VADG$  was expanded to obtain the dose-dependent dose gradient measure  $VADG(D)$  that is analogous to the dose gradient curve of Sung *et al.* [12]. As a result, the  $VADG$  is a function of the absorbed dose  $D$  and can be plotted for the evaluation of dose gradient distributions as a dose-dose gradient function.

It can be demonstrated by means of mathematical considerations and the following results that the

curve characteristic of this function enables qualitative statements about the dose conformity at the target volume's boundary. For better understanding, the steeper the dose gradient curve at the target volume's boundary, the more closely the target volume is encompassed by the isodoses at high dose levels.

### 2.2.4. Algorithms for calculating $VADG$

The algorithms for determining the  $VADG$  were implemented using MATLAB<sup>®</sup> R2007a (The MathWorks, Inc., Natick, MA, USA). The required geometrical and dosimetric input data for the solution of the dose gradient problems came from the utilized treatment planning system. The structure files RS\*.dcm and dose files RD\*.dcm in the DICOM data format were used to calculate the  $VADG$ . The pixel size was  $p_x = p_y \equiv 0.78 \text{ mm}$  in computed axial tomography slices 1 mm thick. The unit cell of the dose grid had side lengths of  $a = b \equiv 0.98 \text{ mm}$  and  $c = 1.00 \text{ mm}$  in the DICOM coordinate directions  $x$ ,  $y$ , and  $z$ .

The algorithm applied for numerical gradient calculation utilizes central (two-sided) differences for interior data points and single-sided differences along the edges of the dose matrix. The step sizes along the positive coordinate axes were constant and identical to the spacing between the data points. The use of central differences obviates the need for additional smoothing.

A mathematical approach will be used for treatment plans with multiple targets to obtain individual values of the  $VADG$  if one isodose of interest encompasses several target volumes. For details, see Subsection 2.2.4 of [16].

### 2.3. Relative errors in dose gradient measures

To quantify the deviations between the approximated dose gradient measures  $X$  and the three-dimensional  $Z = VADG_{proj}$ , the definition

$$\varepsilon(X) = \frac{X - Z}{|Z|} \cdot 100\% \quad (6)$$

of the relative error was used.  $Z$  is the value of the more exact quantity and  $X$  is the value of the approximation. The denominator in Eq. (6) is the absolute value of  $Z$  and is called the reference value. The errors in the two-dimensional dose gradient measures occur due to the linearization in radial direction.

### 2.4. Statistics

Pearson's correlation coefficient  $r$  was used to quantify the strength of a correlation. The probabilities  $p$  of zero correlation were calculated using a one-sided association test based on Student's  $t$  test with  $n - 2$  degrees of freedom, where  $n$  is the sample size. A significance level of  $\alpha = 0.05$  was used and all confidence levels were  $1 - \alpha = 0.95 \hat{=} 95\%$ . The quality of estimating a correlation by a regression function was evaluated using the coefficient of determination  $r^2$  [17].

### 2.5. Treatment and calculation parameters

The possible correlations of the examined dose gradient measures on the  $VADG$  were investigated for the virtual irradiations of 13 spherical brain metastases treated with one single-dose fraction and marginal dose values in a range of 18 to 25 Gy. All of the dose prescriptions strictly comply with the recommendations of the DEGRO Working Group on Stereotactic Radiotherapy [18]. The planning target volume diameters were systematically varied in a range of 3 to 29 mm to achieve steadily decreasing nearly isotropic dose gradients on this variable. For comparability, the same levels of the isodoses of interest were used for the calculation of all of the dose gradient measures: 80% and 40% of the individual maximum dose.

Linac-based stereotactic radiosurgery of 13 brain metastases with a median planning target volume size of 1.60 cm<sup>3</sup> was planned using the treatment planning system iPlan<sup>®</sup> RT Dose 4.5.5 (Brainlab AG, Munich, Germany). All of the planning target

volumes were segmented in the left temporo-parietal hemisphere on the cranial computer tomographs of one patient without lesions. The distance of the geometrical centre of mass of all of the target volumes to the skin was 35 mm. An additional isotropic margin of 0.5 mm was chosen between the planning target volume and the irradiation field aperture. The linear accelerator for the dose delivery as well as the irradiation parameters are specified in [16].

## 3. RESULTS

### 3.1. Best one- and two-dimensional dose gradient measures

One question to be answered is which approximated dose gradient measures describe best almost isotropic three-dimensional dose gradient problems. Table 1 summarizes the ranges, medians, mean values, and standard deviations of the volumes of interest, median dose values within the planning target volume, prescribed isodoses, sample sizes on which the calculations of the anisotropic dose gradient measures were based, and errors in the approximated dose gradient measures relative to the  $VADG_{proj}(NT)|_{D_2}^{D_1}$ . The values of all of the dose gradient measures are shown in Fig. 1.

The errors in the one-dimensional  $SADG^*$  relative to the solution of the three-dimensional dose gradient problem according to Eq. (2) showed a range of 22.1% (median of -4.6%). A comparison of the errors in the two-dimensional dose gradient measures revealed the worst range of 22.3% (median of -7.4%) in the  $SADG$  and the best range of 5.2% (median of -10.8%) in the  $SADG_{RD}$ . The errors in the three-dimensional  $VADG_{min}$  also showed a range of 5.2% (median of -3.9%).

The errors in the  $SADG_{RD}$  relative to the  $VADG_{proj}$  occurred due to the linearization, whereas the reduction factor of the median sample size was  $1\ 128/6\ 143 = 1/5.4$  (see Table 1). The ranges of the errors and reduction factors for the six brain metastases treated by the circular cones were -14.8 to -10.3% (median of -11.2%) and 1/7.5 to 1/5.1 (median of 1/6.5), respectively. The corresponding values for the eight lesions treated by the multi-leaf collimator were -11.5 to -9.6% (median of -10.7%) and 1/5.5 to 1/4.7 (median of 1/5.1), respectively.

**Table 1.** Sizes of the target volumes, median dose values, prescribed isodose levels, volumes of the isodoses of interest, sample sizes, and relative errors in the approximated dose gradient measures for the stereotactic radiosurgery of 13 brain metastases treated with one single-dose fraction.  $d_{PTV}$  diameter of the planning target volume;  $V_{PTV}$  size of the planning target volume;  $D_{50\%}$  median dose within the planning target volume;  $D_{PI(PTV)}$  level of the prescribed isodose at the planning target volume's boundary;  $V(D_1)$  volume within the isodose at level  $D_1 \equiv D_{PI(PTV)} = 80\%$  relative to the maximum dose;  $V(D_2)$  volume within the isodose at level  $D_2 = 40\%$  relative to the maximum dose;  $n(Y)$  sample sizes of  $Y \in \{SADG, SADG_{RD}, VADG_{min}, VADG_{proj}\}$ ;  $SADG, SADG_{RD}$  superficially averaged dose gradients;  $VADG_{min}, VADG_{proj}$  minimal and radially projected volumetrically averaged dose gradients;  $NT$  nonspecific normal tissue;  $\varepsilon(Z)$  errors in  $Z \in \{SADG^*, \overline{\Delta r_{\Delta D}}, SADG, SADG_{RD}, VADG_{min}\}$  relative to  $VADG_{proj}$  according to Eq. (6);  $SADG^*$  spatially averaged dose gradient;  $\overline{\Delta r_{\Delta D}}$  superficially averaged radius difference. <sup>a</sup>An isotropic safety margin of 1 mm was chosen between the gross tumour volume and planning target volume. <sup>b</sup>Valid for  $VADG_{min}$  and  $VADG_{proj}$ .

Quantity [Unit]	Minimum	Maximum	Median	Mean value	Standard deviation
$d_{PTV} [mm]^a$	3.0	29.0	14.5	15.4	8.0
$V_{PTV} [cm^3]$	0.01	12.77	1.60	3.37	3.98
$D_{50\%} [Gy]$	20.9	29.1	23.6	24.1	2.6
$D_{PI(PTV)} [Gy]$	18.0	25.0	20.0	20.6	2.2
$V(D_1) [cm^3]$	0.01	12.92	1.64	3.41	4.05
$V(D_2) [cm^3]$	0.08	31.65	5.24	8.87	9.94
$n[SADG(NT) _{D_2}^{D_1}] [1]$	201	7 318	2 147	2 511	2 460
$n[SADG_{RD}(NT) _{D_2}^{D_1}] [1]$	20	7 196	1 128	1 979	2 265
$n[VADG(NT) _{D_2}^{D_1}] [1]^b$	143	34 058	6 143	9 811	10 622
$\varepsilon(SADG^* _{D_2}^{D_1}) [\%]$	-18.9	3.2	-4.6	-6.8	7.7
$\varepsilon[\overline{\Delta r_{\Delta D}}(NT) _{D_2}^{D_1}] [\%]$	-17.2	1.5	-6.9	-7.2	6.3
$\varepsilon[SADG(NT) _{D_2}^{D_1}] [\%]$	-20.8	1.5	-7.4	-8.2	7.4
$\varepsilon[SADG_{RD}(NT) _{D_2}^{D_1}] [\%]$	-14.8	-9.6	-10.8	-11.1	1.3
$\varepsilon[VADG_{min}(NT) _{D_2}^{D_1}] [\%]$	-6.6	-1.4	-3.9	-3.5	1.8

### 3.2. Correlation analyses between dose gradient measures

The  $VADG_{proj}(NT)|_{D_2}^{D_1}$  was picked out of the set of 16 different dose gradient measures to be the reference variable for the correlation analyses between the dose gradient measures. The objective of these analyses is to find the dose gradient measures with the strongest and weakest correlations on the mean value of the physical dose gradients.

The correlations and regression lines of 15 dose gradient measures and the values of Pearson's correlation coefficient  $r$  are presented in Fig. 1 and Table 2. The regression lines on the left side in the subplots of Fig. 1 appertain to the smaller planning target volumes with diameters between 3 and 14 mm treated with circular cones; the larger diameters between 14 and 29 mm with the regression lines on the right side were treated with the multi-leaf collimator.

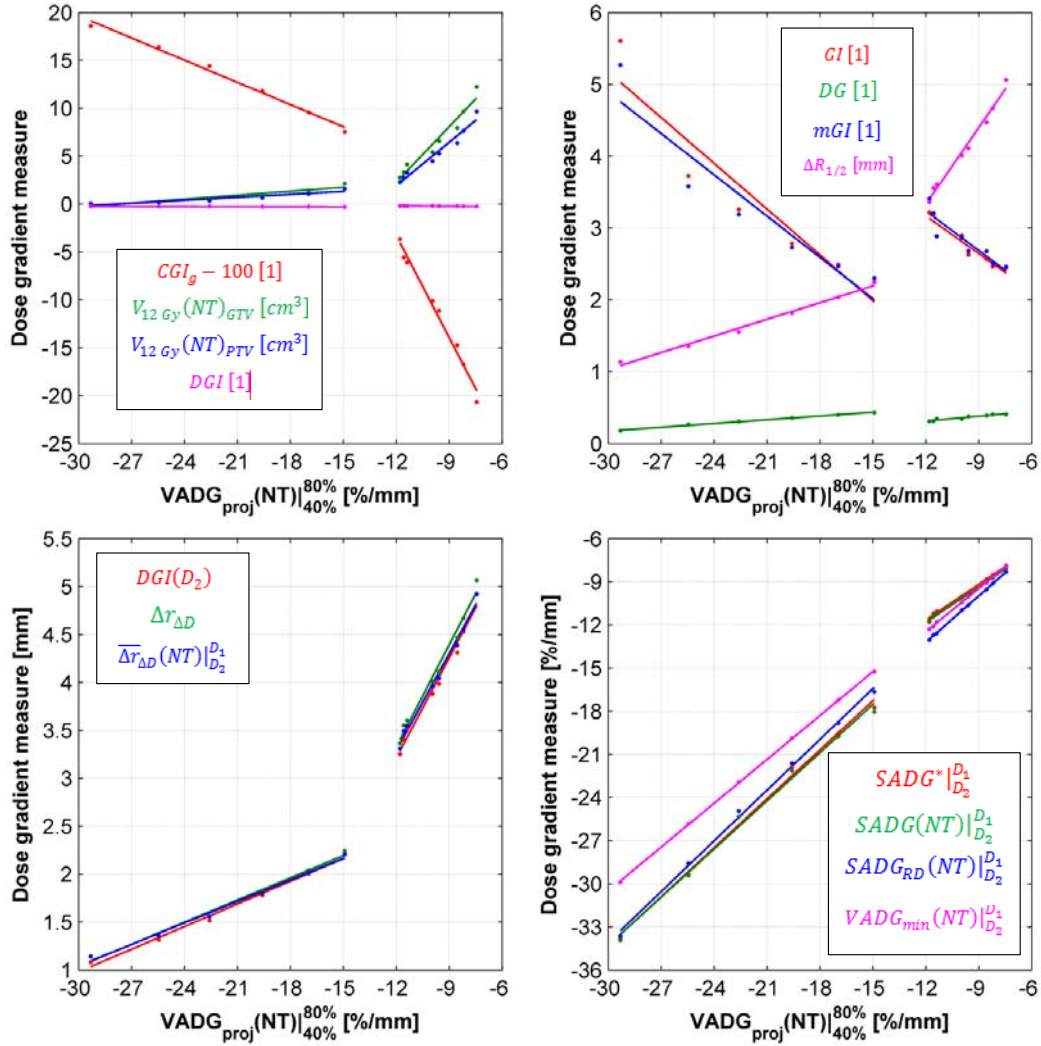


**Fig. 1.** Correlations and regression lines  $y = a \cdot x + b$  of 15 different dose gradient measures on  $x = VADG_{proj}(NT)|_{40\%}^{80\%}$  for the stereotactic radiosurgery of 13 brain metastases treated with one single-dose fraction. For abbreviations of the dose gradient measures, see the following references:  $CGI_g$  [14];  $V_{12 Gy}(Brain)$  [5, 6];  $DGI$  [10];  $GI$  [4];  $DG$  [15];  $mGI$  [8];  $\Delta R_{1/2}$  [11];  $DGI(D_2)$  [12];  $\Delta r_{\Delta D}$  [13];  $\overline{\Delta r_{\Delta D}}(NT)$ , see Eq. (A.4);  $SADG^*|_{D_2}^{D_1}$  [13];  $SADG(NT)|_{D_2}^{D_1}$ , see Eq. (A.1);  $SADG_{RD}(NT)|_{D_2}^{D_1}$ , see Appendix A.1;  $VADG_{min}(NT)|_{D_2}^{D_1}$  minimal volumetrically averaged dose gradient for the normal tissue  $NT$  between the isodoses of interest at the levels  $D_1 = 80\%$  and  $D_2 = 40\%$  relative to the maximum dose within the planning target volume, see Subsection 2.2.1;  $VADG_{proj}(NT)|_{D_2}^{D_1}$  radially projected volumetrically averaged dose gradient according to Eq. (2).

In the group of the one-dimensional dose gradient measures, the  $SADG^*|_{D_2}^{D_1}$  showed the strongest correlations on the  $VADG_{proj}(NT)|_{D_2}^{D_1}$  for both collimation types with  $r \geq 0.997$  and  $p \leq 1.4 \cdot 10^{-5}$ . The weakest correlations with the  $VADG_{proj}(NT)|_{D_2}^{D_1}$  had  $V_{12 Gy}(NT)$ ,  $GI$ ,  $mGI$ , and  $DGI$  with  $|r| \in [0.906, 0.978]$  and  $p \in [2.5 \cdot 10^{-5}, 5.7 \cdot 10^{-3}]$ .

From all of the two-dimensional dose gradient measures, the  $SADG_{RD}(NT)|_{D_2}^{D_1}$  showed the strongest correlations on the reference variable with  $r \geq 0.999$  and  $p \leq 2.1 \cdot 10^{-6}$ . The  $SADG(NT)|_{D_2}^{D_1}$  and  $\overline{\Delta r_{\Delta D}}(NT)|_{D_2}^{D_1}$  had also strong correlations with the  $VADG_{proj}(NT)|_{D_2}^{D_1}$ :  $r \geq 0.994$  and  $p \leq 2.0 \cdot 10^{-5}$ .

**Table 2.** Correlation parameters of 15 different dose gradient measures on the  $VADG_{proj}(NT)|_{D_2}^{D_1}$  for the stereotactic radiosurgery of 13 brain metastases treated with one single-dose fraction.  $r$  Pearson's correlation coefficient;  $p$  probability of zero correlation;  $\|\nabla \cdot D(\mathbf{r})\|$   $\nearrow$  increasing dose gradient magnitude;  $D_1 = 80\%$  isodose of interest at the upper level;  $D_2 = 40\%$  isodose of interest at the lower level;  $\nearrow$  increasing dose gradient measure;  $\searrow$  decreasing dose gradient measure;  $V_{PTV}$  size of the planning target volume. For abbreviations of the dose gradient measures, see the following references:  $CGI_g$  [14];  $V_{12 Gy}(Brain)_{GTV}$  [5, 6];  $GI$  [4];  $DG$  [15];  $mGI$  [8];  $DGI$  [10];  $\Delta R_{1/2}$  [11];  $DGI(D_2)$  [12];  $\Delta r_{\Delta D}$  [13];  $SADG^*|_{D_2}^{D_1}$  [13];  $\overline{\Delta r_{\Delta D}}(NT)|_{D_2}^{D_1}$ , see Eq. (A.4);  $SADG(NT)|_{D_2}^{D_1}$ , see Eq. (A.1);  $SADG_{RD}(NT)|_{D_2}^{D_1}$ , see Appendix A.1;  $VADG_{min}(NT)|_{D_2}^{D_1}$  minimal volumetrically averaged dose gradient, see Subsection 2.2.1. <sup>a</sup>Or the equivalent trend on  $V_{PTV}$   $\searrow$  because the course of  $VADG_{proj}(NT)|_{D_2}^{D_1}$  on  $V_{PTV}$  is strictly monotonically increasing. <sup>b</sup>False trend compared to the intention of the dose gradient metric's authors.

Collimation type	Circular cones		Multi-leaf collimator		Both
	$r$ [1]	$p$ [1]	$r$ [1]	$p$ [1]	
Dose gradient measure					Trend on $\ \nabla \cdot D(\mathbf{r})\ $ $\nearrow^a$
$CGI_g$	-0.995	$3.4 \cdot 10^{-5}$	-0.992	$1.4 \cdot 10^{-6}$	$\nearrow$
$V_{12 Gy}(Brain)_{GTV}$	0.938	$5.7 \cdot 10^{-3}$	0.976	$3.4 \cdot 10^{-5}$	$\searrow$
$V_{12 Gy}(Brain)_{PTV}$	0.940	$5.4 \cdot 10^{-3}$	0.978	$2.5 \cdot 10^{-5}$	$\searrow$
$GI$	-0.942	$5.0 \cdot 10^{-3}$	-0.942	$4.6 \cdot 10^{-4}$	$\nearrow^b$
$DG$	0.997	$1.7 \cdot 10^{-5}$	0.954	$2.4 \cdot 10^{-4}$	$\searrow^b$
$mGI$	-0.944	$4.7 \cdot 10^{-3}$	-0.915	$1.4 \cdot 10^{-3}$	$\nearrow^b$
$DGI$	-0.947	$4.2 \cdot 10^{-3}$	-0.906	$1.9 \cdot 10^{-3}$	$\nearrow^b$
$\Delta R_{1/2}$	0.995	$3.4 \cdot 10^{-5}$	0.992	$1.4 \cdot 10^{-6}$	$\searrow$
$DGI(D_2)$	0.996	$2.5 \cdot 10^{-5}$	0.991	$2.0 \cdot 10^{-6}$	$\searrow$
$\Delta r_{\Delta D}$	0.995	$3.7 \cdot 10^{-5}$	0.992	$1.3 \cdot 10^{-6}$	$\searrow$
$SADG^* _{D_2}^{D_1}$	0.997	$1.4 \cdot 10^{-5}$	0.998	$9.5 \cdot 10^{-9}$	$\searrow$
$\overline{\Delta r_{\Delta D}}(NT) _{D_2}^{D_1}$	0.996	$2.0 \cdot 10^{-5}$	0.994	$5.1 \cdot 10^{-7}$	$\searrow$
$SADG(NT) _{D_2}^{D_1}$	0.996	$1.9 \cdot 10^{-5}$	0.999	$6.6 \cdot 10^{-9}$	$\searrow$
$SADG_{RD}(NT) _{D_2}^{D_1}$	0.999	$2.1 \cdot 10^{-6}$	1.000	$6.3 \cdot 10^{-11}$	$\searrow$
$VADG_{min}(NT) _{D_2}^{D_1}$	1.000	$6.6 \cdot 10^{-9}$	1.000	$8.7 \cdot 10^{-11}$	$\searrow$

The trends in 15 dose gradient measures on an increasing value of the reference variable were also examined. The dose gradient indices  $GI$ ,  $DG$ ,  $mGI$ , and  $DGI$  showed false positive trends on the  $VADG_{proj}(NT)|_{D_2}^{D_1}$  as shown in Fig. 1 and Table 2. Although Fig. 1 shows constant regression lines for the  $DGI$  because of the large scale of the

ordinate,  $r \leq -0.906$  in Table 2 indicates the false positive trends.

### 3.3. Graphical representations of dose gradients

In this section, three different visualizations of the dose gradients in space will be presented for one brain metastasis with the planning target volume

diameter 29 mm and irradiated by means of the multi-leaf collimator: the transversal vector field of the dose gradients, the dose gradient-frequency histogram, and the dose-dependent dose gradient function.

### 3.3.1. Vector fields of dose gradients

Fig. 2 represents one two-dimensional distribution of the dose gradients in the isocentric axial plane with isodose lines in 2 Gy steps in a range of 8 to 22 Gy. The black arrows represent the dose gradient vectors  $\nabla \cdot D(x, y, z = 0 \text{ mm})$  and point in the direction of decreasing dose. The distances between all pairs of isodose lines and the vector lengths are functions on the circumferential angle. This verifies the anisotropy of the dose gradient problem although the magenta circular disc represents a globular planning target volume.

The non-zero vector lengths within the isodose line at level 18 Gy in Fig. 2 indicate the dose inhomogeneity within the planning target volume. The range and median of the dose gradient magnitudes within the planning target volume were calculated: -3.8 to 3.5 Gy/mm and 0.0 Gy/mm, respectively. The signed dose gradient magnitudes in space for all of the eight brain metastases treated by the multi-leaf collimator were in a range of -5.0 to 5.1 Gy/mm (median range of -4.2 to 4.4 Gy/mm). The corresponding values of the homogeneity index *HI* according to ICRU Report 83 [2] were in a range of 0.19 to 0.21 (median of 0.20). Otherwise, the dose gradient magnitudes for all of the six lesions treated by the circular cones were in a range of -9.5 to 10.1 Gy/mm (median range of -8.0 to 7.3 Gy/mm). The corresponding values of the *HI* were in a range of 0.17 to 0.27 (median of 0.22). Therefore, the narrower the range of the dose gradient magnitudes within the planning target volume, the better is the dose homogeneity.

In addition to the type of vector field shown in Fig. 2, the VADG algorithm can calculate and display coronal, sagittal, and three-dimensional vector fields of the dose gradients.

### 3.3.2. Dose gradient-frequency histogram

Fig. 3 represents one differential dose gradient-frequency histogram of the negative magnitude of the dose gradient  $-\|\nabla \cdot D(NT)_{40\%}^{80\%}\|_{proj}$  according

to Eq. (1) with two measures of the location and two of the shape: median, modal value, skewness, and kurtosis.

The median of -7.2%/mm is the abscissa value of the geometrical centre of mass of the frequency distribution. The median values for all of the eight brain metastases treated by the multi-leaf collimator were in a range of -11.8 to -7.2%/mm (median of -9.7%/mm). The range and median of the median values for all of the six lesions treated by the circular cones were -29.9 to -15.2%/mm and -21.7%/mm, respectively.

The modal value and the abscissa value of the absolute maximum of the distribution were equal to -9.1%/mm. All of the eight modal values for the brain metastases treated by the multi-leaf collimator were in a range of -12.8 to -8.2%/mm (median of -9.1%/mm). The corresponding values for the six lesions treated by the circular cones were -29.3 to -18.9%/mm and -22.7%/mm, respectively.

The negative skewness  $g_1 = -0.193$  suggested that the frequency distribution in Fig. 3 is left-skewed. The range of the eight values of  $g_1$  for the lesions treated by the multi-leaf collimator was -0.193 to 0.060 (median of -0.023). The corresponding values for the six lesions treated by the circular cones were 0.027 to 1.130 and 0.505, respectively. All of the frequency distributions of the dose gradients generated through the circular cones were right-skewed – contrary to the dose gradient distributions generated through the multi-leaf collimator.

Furthermore, the distribution in Fig. 3 was with the negative kurtosis  $g_2 = -0.504$  broader and more platykurtotic than the Gaussian bell curve of the normal distribution. The eight values of  $g_2$  for the brain metastases treated by the multi-leaf collimator were in a range of -0.669 to -0.066 (median of -0.510). The corresponding values for the six lesions treated by the circular cones were -0.812 to 3.075 and 0.358, respectively. All of the frequency distributions of the dose gradients generated through the multi-leaf collimator were platykurtotic – contrary to the some leptokurtotic dose gradient distributions generated through the circular cones.

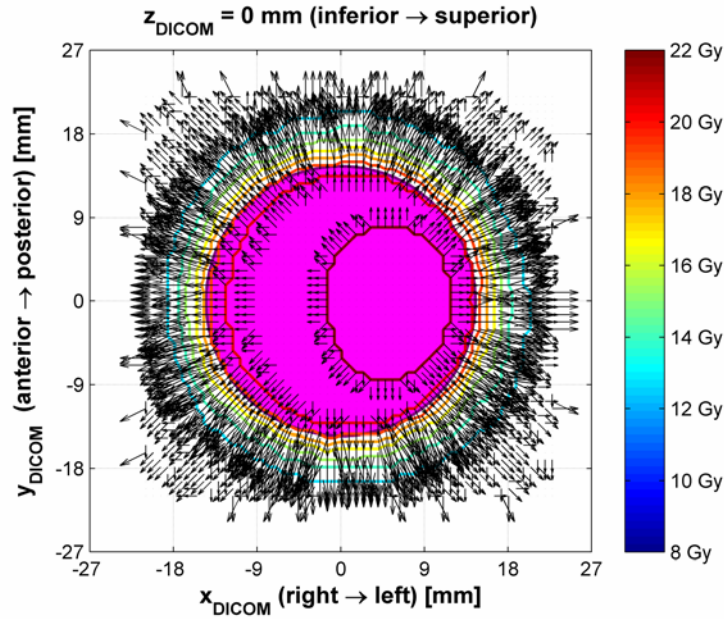


**Fig. 2.** Isocentric axial section through the vector field of dose gradients with isodose lines for the stereotactic radiosurgery of one brain metastasis with 29 mm planning target volume diameter and irradiated through the multi-leaf collimator. The black arrows are the dose gradient vectors; the magenta circular disc represents the cross sectional area of the planning target volume; eight different isodose lines at the levels (8 : 2 : 22) Gy;  $\{ISO, x, y, z\}$  DICOM coordinate system, see Subsection 2.2;  $ISO$  isocentre.

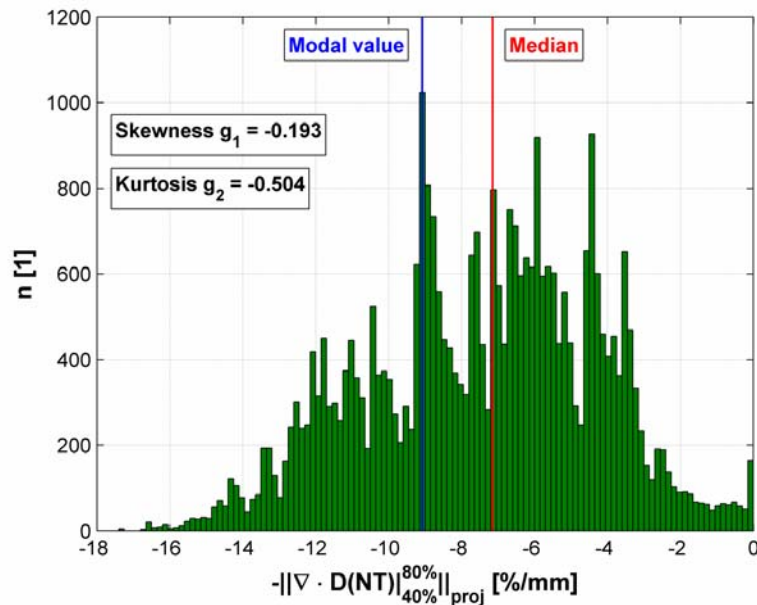


**Fig. 3.** Differential dose gradient-frequency histogram for the nonspecific normal tissue with the statistical values median and modal value of the dose gradients and the measures of the shape skewness and kurtosis for the stereotactic radiosurgery of the lesion shown in Fig. 2.  $-\|\nabla \cdot D(NT)\|_{40\%}^{80\%} / proj$  negative magnitude of a dose gradient towards the nonspecific normal tissue; class width of 0.15%/mm;  $NT$  nonspecific normal tissue;  $n$  frequency; for the definitions of skewness and kurtosis, see [17].

### 3.3.3. Dose-dependent dose gradient function

Fig. 4 shows one curve characteristic of the dose-dose gradient function that was calculated using the VADG formalism according to Subsections 2.2.3 and 2.2.4. The regression curve represents the characteristics of the VADG on the absorbed dose  $D$  outside the planning target volume with 29 mm diameter. The coefficients of the sixth degree polynomial were  $a_6 = -2.2 \cdot 10^{-6} \text{Gy}^{-5} \cdot \text{mm}^{-1}$ ,  $a_5 = 1.3 \cdot 10^{-4} \text{Gy}^{-4} \cdot \text{mm}^{-1}$ ,  $a_4 = -2.9 \cdot 10^{-3} \text{Gy}^{-3} \cdot \text{mm}^{-1}$ ,  $a_3 = 3.0 \cdot 10^{-2} \text{Gy}^{-2} \cdot \text{mm}^{-1}$ ,  $a_2 = -1.6 \cdot 10^{-1} (\text{Gy} \cdot \text{mm})^{-1}$ ,  $a_1 = 2.6 \cdot 10^{-1} \text{mm}^{-1}$ , and  $a_0 = -1.7 \cdot 10^{-1} \text{Gy} / \text{mm}$ .

The maximal steepness of the curve  $VADG_{min}(D)$  at the target volume's boundary is a measure for the local dose conformity. The maximum slope at the prescribed dose  $D_{PI} = 18 \text{Gy}$  was  $0.3 \text{mm}^{-1}$  as shown in Fig. 4. The range and median of this quantity for all of the eight brain metastases treated by the multi-leaf collimator were  $0.3$  to  $0.7 \text{mm}^{-1}$  and  $0.5 \text{mm}^{-1}$ , respectively. The corresponding values of Paddick's conformity index  $PCI_{PI}$  [19] at the prescribed isodose level were in a range of  $0.70$  to  $0.92$  (median of  $0.85$ ). Otherwise, the maximum slopes for all of the six lesions treated by the circular cones were in a range of  $0.8$  to  $1.3 \text{mm}^{-1}$  (median of  $1.1 \text{mm}^{-1}$ ). The corresponding values of the  $PCI_{PI}$  were in a range of  $0.66$  to  $0.98$  (median of  $0.92$ ). Therefore, the steeper the curve  $VADG_{min}(D)$  at the dose level  $D_{PI}$ , the better is the dose conformity to the planning target volume.

### 3.4. Computation time

The computation time  $t_{CPU}$  for the calculation of the VADG was in a range of  $57 \text{s}$  to  $25 \text{min } 39 \text{s}$  on a personal computer with a single-core processor speed of  $2 \text{GHz}$  and random access memory of  $1 \text{918 Mbytes}$ .  $t_{CPU}$  was dependent on the sample size  $n(\nabla \cdot D)$  of the included dose gradients that was in a wide range of  $143$  to  $34 \text{058}$ . An adequate corresponding regression function with  $r^2 = 1.000$  is a third degree polynomial with the coefficients  $a_3 = 1.2 \cdot 10^{-12} \text{min}$ ,  $a_2 = -2.8 \cdot 10^{-8} \text{min}$ ,  $a_1 = 3.0 \cdot 10^{-4} \text{min}$ , and  $a_0 = -4.9 \cdot 10^{-2} \text{min}$ .

### 3.5. Classification of VADG

The new VADG is an explicit three-dimensional dose gradient measure that directly quantifies

dose gradients and has the unit  $\text{Gy}/\text{mm}$  or  $\%/ \text{mm}$ . Moreover, it is perfectly flexible in defining the levels of the isodoses of interest, shows true trends on a varying mean value of the dose gradients, is applicable to treatment plans with multiple targets, and is independent of the size and form of the target volume. There are no restrictions regarding comparisons between different patients, irradiation series, treatment techniques, and treatment modalities concerning the dose gradients. Nevertheless, the computational expense is huge.

## 4. DISCUSSION

### 4.1. Quality of approximated dose gradient measures

From all of the one-dimensional dose gradient measures, the approximated  $SADG^*|_{D_2}^{D_1}$  was superior to the common dose gradient indices with regard to both the maximal errors relative to  $VADG_{proj}(NT)|_{D_2}^{D_1}$  and the strongest correlations on  $VADG_{proj}(NT)|_{D_2}^{D_1}$ . In this respect, the  $SADG_{RD}$  is the best two-dimensional dose gradient measure to describe three-dimensional dose gradient distributions.

The regression lines in Fig. 1 to describe the trends in  $V_{12 \text{Gy}}(NT)$ ,  $GI$ , and  $mGI$  on the  $VADG_{proj}(NT)|_{D_2}^{D_1}$  are merely rough approximations.

Hence, the qualitative and quantitative comparability of mean values of the physical dose gradients by means of these one-dimensional dose gradient indices is limited. A reduced comparability of irradiation series in terms of dose gradients is the clinical consequence from that.

The gaps between the regression lines in the subplots of Fig. 1 between  $-15$  and  $-12\%/ \text{mm}$  and at  $d_{PTV} = 14 \text{mm}$  were caused by the change in the collimation type. The physical penumbra of the  $15 \text{mm}$  circular cone is smaller than that of the also utilized irradiation field aperture of the same size and formed by the multi-leaf collimator because of different transmissions and geometries due to the finite isocentric leaf width of  $2.5 \text{mm}$ .

The errors in the  $VADG_{min}$  relative to the  $VADG_{proj}$  result from differences in the directions of the dose gradient vectors: The  $VADG_{min}$  includes the magnitudes of the steepest dose gradients, and the calculation of the  $VADG_{proj}$  takes into account the radial projections of the

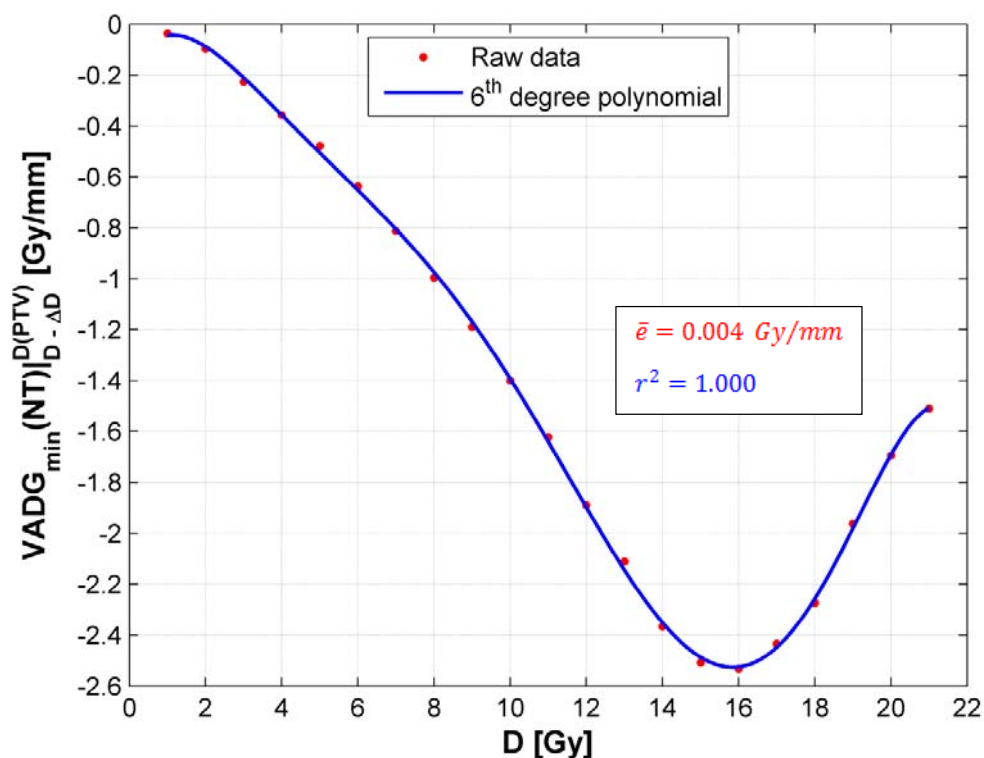


**Fig. 4.** Dose gradient function at the target volume's boundary on the absorbed dose for the stereotactic radiosurgery of the lesion shown in Fig. 2.  $VADG_{\min}(NT)|_{D-\Delta D}^{D(PTV)}$  minimal volumetrically averaged dose gradient according to Subsection 2.2.1;  $NT$  nonspecific normal tissue;  $D(PTV) \leq 21$  Gy absorbed dose at target volume's boundary;  $D \in [1, 21]$  Gy upper level of an isodose surface for calculating the dose gradients;  $\Delta D = 1$  Gy dose increment for calculating the dose gradients;  $\bar{e} = \sqrt{\sum_{i=1}^n e_i^2/n}$  mean value of the residuals;  $n = 21$  number of sampling points;  $r^2$  coefficient of determination, see [17].

dose gradients. They were small because the dose gradient distributions at the boundary of the spherical planning target volumes were nearly isotropic. The advantages and disadvantages of both three-dimensional dose gradient measures will be discussed in a forthcoming article that addresses descriptions of more anisotropic dose gradient distributions at the boundary of irregularly formed target volumes.

#### 4.2. Loss of accuracy due to linearization

The loss of accuracy due to the linearization of the dose gradients by the difference quotients was demonstrated in the values of the errors in the  $SADG_{RD}$  relative to the  $VADG_{proj}$  as shown in Table 1. The  $SADG_{RD}$  is a two-dimensional dose gradient measure, and the  $VADG_{proj}$  is three-dimensional; but both are determined using the

dose matrix. The error ranges in the  $SADG_{RD}$  as well as the median reduction factors of the sample sizes in the last paragraph of Subsection 3.1 had different values for the collimation types circular cones and multi-leaf collimator: 4.5% versus 1.9% and 1/6.5 versus 1/5.1, respectively. Thus, the smaller the sample size of a dose gradient problem, the greater the loss of accuracy due to the linearization.

Another impact on the loss of accuracy due to the linearization is the dose difference between the isodoses of interest. The linearization errors will increase with a growing dose difference because the uniformity of the dose gradients is best within the photon beam penumbra defined between the isodose levels 20% and 80% relative to the central axis intensity and will be violated more and more at lower and higher dose levels.

### 4.3. Need for anisotropic dose gradient measures and information content of histograms

The generation of locally steep dose gradients towards the organs at risk with photon beams and the use of asymmetric field alignments result in isodose surfaces that are more irregular than the planning target volume. Even the isodoses around the spherical target volumes were not exactly globular after the optimisation of the beam geometry. The frequency distributions of the dose gradients in wide value ranges were irregularly formed (see Fig. 3). Consequently, all of the clinical dose gradient problems are anisotropic. The physical reason: Centrally symmetric dose distributions with isotropic dose gradients are impossible in teletherapy of lesions in humans.

The frequency distribution of the three-dimensional dose gradients shown in Fig. 3 is more irregular than the solid angle distribution of the two-dimensional dose difference quotients that are included in the *SADG*; see also Fig. 4b in [16]. The *VADG* provides more information on anisotropic dose gradient distributions than the *SADG* because it is the solely three-dimensional dose gradient measure.

The four histogram parameters median, modal value, skewness, and kurtosis are helpful for evaluating the global dose gradient conditions. The smaller the median and modal value of the dose gradients, the better the restriction of the absorbed dose to the nonspecific normal tissue and the organs at risk. An increasing skewness has the same effects when the frequency distribution on the dose gradient becomes more right-skewed. The higher the value of the kurtosis, the more homogeneous is the dose gradient distribution at the target volume's boundary. Conversely, the smaller the kurtosis, the better the dose fall-off towards one or more organs at risk.

### 4.4. Requirements of dose gradient measures

The features of a good dose gradient measure are specified in [16]. In this context, the definition of the *VADG* according to Eq. (2) is universal such that the lower isodose levels can be adapted to the tolerance dose values of the involved tissue types. Additionally, the *VADG* fulfils all of the requirements specified in [16] except for the simplicity of definition and rapid calculation results. High computational expense is one drop

of bitterness with respect to the determination of all of the multi-dimensional dose gradient measures. The additional computation time taking the third dimension into account is enormous for large dose gradient problems: > 25 min (see Subsection 3.4) versus < 1 min for calculating the *SADG* [16].

The analyses of clinically validated correlations between complication rates and the values of the multi-dimensional dose gradient measures have to be conducted for various tumour entities. The *SADG* and *VADG* have through the exact description of dose gradient distributions the best prerequisites to pass these clinical tests. The author will present strong correlations between global and local values of both dose gradient measures on dosimetric quantities in healthy tissue in a forthcoming article.

If the algorithm for the calculation of the *VADG* was implemented in all of the existing treatment planning systems, the utilization of this dose gradient measure would be easy for all users. The maximal computation time given in Subsection 3.4 can drastically be reduced by use of a workstation of the latest generation. The additional computational expense is acceptable compared to the time required for three-dimensional dose calculations using advanced algorithms based on the Monte Carlo method and the explicit solution of the linearized Boltzmann transport equation.

### 4.5. Outlook and vision

Application possibilities of the *VADG* are or could be:

- With the inclusion of dose conformity and homogeneity in the *VADG* formalism noted in Subsections 3.3.1 and 3.3.3, dose distributions in the region of the target volume can be optimised with respect to these quality criteria.
- Reassurance of dose distributions with optimal dose fall-off towards the organs at risk based on a comparison with the physically achievable dose gradients dependent on the treatment parameters that influence the total penumbra. For a better understanding, irradiation machines do not deliver organ dose values but dose profiles with well-known dose gradients at the field limits.
- Implementation of the *VADG* algorithm in existing treatment planning systems to solve

anisotropic dose gradient problems with large and irregularly formed target volumes – not only with stereotactic targets.

- The VADG algorithm should be implemented in existing patient plan verification systems to support the gamma index analysis by the comparison of the calculated with measured dose gradients in high dose gradient regions.

## 5. CONCLUSION

The *VADG* is a new explicit and three-dimensional description of anisotropic dose gradient distributions. Except little computational expense and proven clinical validity, it possesses all of the features of good dose gradient measures as listed in Subsection 4.4. The values of the dose gradients for each lesion varied within wide ranges in the irradiation series for 13 spherical brain metastases. This circumstance and the loss of accuracy due to the linearization in the *SADG* reinforced the need for three-dimensional dose gradient measures. The *VADG* is a logical advancement of the *SADG*. The graphical representations of the dose gradients in the forms of vector fields, dose gradient-frequency histograms, and dose-dependent dose gradient functions with their descriptive parameters are helpful for evaluating the global and local dose gradient distributions.

The algorithm for determining the *VADG* based on the vector field of the dose gradients can also take into account the dose homogeneity and conformity within and at the boundary, respectively, of the target volume. The calculation of the *VADG* should be implemented in existing

treatment planning systems. Additionally, the VADG algorithm in patient plan verification systems could compare locally calculated and measured dose gradients. All of the one- and two-dimensional dose gradient measures are now verifiable by means of the VADG formalism. Through the *VADG*, one is able to investigate the impacts of different collimators and collimation types on the dose fall-off at the target volume's boundary.

The results of the performed correlation analyses again revealed the shortcomings of the dose gradient indices recommended in ICRU Report 91 that were not mentioned in [3] and the review article [20]. Especially the *GI* and other dose gradient indices based on volume ratios of the isodoses of interest should no longer be used because of false trends on the physical dose gradient and severely limited comparability of its values in terms of dose gradients.

## FUNDING

No funding at all has been claimed for this study.

## CONFLICT OF INTEREST STATEMENT

Markus Wösle declares that he has no competing interests.

## APPENDIX

### A.1. Superficially averaged dose gradient

The mathematical formulations of the linearized two-dimensional anisotropic dose gradient problem for the nonspecific normal tissue (*NT*) and an arbitrary organ at risk (*OAR<sub>i</sub>*)

$$SADG(X)|_{D_2}^{D_1} = \frac{1}{\Omega_X} \cdot \int_{(\varphi_X)} \int_{(\vartheta_X)} \frac{D_2 - D_1}{r_2(\varphi, \vartheta) - r_1(\varphi, \vartheta)} \cdot \sin \vartheta \cdot d\vartheta \cdot d\varphi \in \mathbb{R}^-, \quad X \in \{NT, OAR_i\} \quad (A.1)$$

are quotients of surface integrals of the difference quotient  $\Delta D/\Delta r$  and solid angles. The underlying system of coordinates  $K_S = \{O, r, \varphi, \vartheta\}$  has been explained in Subsection 2.2. Eq. (A.1) is the result of applying the generalised first mean value theorem for integration to the surface integrals; see also [21].

The anisotropic radii  $r_1$  and  $r_2$  are the lengths of the position vectors to the surface points of the isodoses of interest. Their dose levels  $D_1$  and  $D_2$  define the surfaces of the treated and irradiated volumes, respectively. The infinitesimal surface element and solid angle element of the unit sphere are  $dS = \sin \vartheta \cdot d\vartheta \cdot d\varphi = d\Omega$  with which the

difference quotient must be integrated. For the nonspecific normal tissue, the integration range is the entire solid angle  $\Omega_{NT} = 4 \cdot \pi$  sr with the angle ranges  $\varphi_{NT} = [0, 2 \cdot \pi]$  and  $\vartheta_{NT} = [0, \pi]$ . For each

organ at risk, the individual segment  $\Omega_{OAR_i}$  of the entire solid angle is defined by the angle ranges  $\varphi_{OAR_i}$  and  $\vartheta_{OAR_i}$ :

$$(\varphi_{OAR_i}, \vartheta_{OAR_i}) = \{(\varphi, \vartheta) \mid t \cdot \mathbf{r}(\varphi, \vartheta) \in V_{OAR_i}\}, \quad \mathbf{r} = (x, y, z)^T, \quad t \in \mathbb{R}^+. \quad (\text{A.2})$$

The radius vectors  $\mathbf{r}$  are written in Cartesian coordinates of the system  $K_C = \{O, x, y, z\}$ , for example, DICOM coordinates; see also Subsection 2.2.  $t$  is a real positive number, and  $V_{OAR_i}$  is the volume of  $OAR_i$ . The individual solid angle

$$\Omega_{OAR_i} = \int_{(\varphi_{OAR_i})} \int_{(\vartheta_{OAR_i})} dS \in \mathbb{R}^+ \quad (\text{A.3})$$

follows from the application of the results of Eq. (A.2) to the definition of the solid angle [16].

All of the needed input data are content of the structure file RS\*.dcm from the utilized treatment planning system. The *SADG* values can also be calculated using the dose matrix in the dose file RD\*.dcm from the utilized treatment planning system. For distinctiveness of the basic input data, the quantity *SADG<sub>RD</sub>* receives the input file type as a subscript [16].

## A.2. Superficially averaged radius difference

The superficially averaged radius difference

$$\overline{\Delta r_{\Delta D}(X)}|_{D_2}^{D_1} = \frac{D_2 - D_1}{SADG(X)|_{D_2}^{D_1}} \in \mathbb{R}^+, \quad X \in \{NT, OAR_i\} \quad (\text{A.4})$$

is a result of applying the definition of the difference quotient  $\Delta D / \Delta r = (D_2 - D_1) / (\bar{r}_2 - \bar{r}_1)$  on the results of Eq. (A.1); it is itself a dose gradient measure [16].

## REFERENCES

1. Landberg, T., Chavaudra, J., Dobbs, J., Gerard, J. P., Hanks, G., Horiot, J. C., Johansson, K. A., Möller, T., Purdy, J., Suntharalingam, N. and Svensson, H. 1999, J. Int. Comm. Radiat. Units Meas., 32, 1.

2. International Commission on Radiation Units and Measurements 2010, J. Int. Comm. Radiat. Units Meas., 10, 1.
3. International Commission on Radiation Units and Measurements 2014, J. Int. Comm. Radiat. Units Meas., 14, 1.
4. Paddick, I. and Lippitz, B. 2006, J. Neurosurg. (Suppl.), 105, 194.
5. Flickinger, J. C., Kondziolka, D., Lunsford, L. D., Kassam, A., Phuong, L. K., Liščák, R. and Pollock, B. 2000, Int. J. Radiat. Oncol. Biol. Phys., 46, 1143.
6. Korytko, T., Radivoyevitch, T., Colussi, V., Wessels, B. W., Pillai, R., Maciunas, R. J. and Einstein, D. B. 2006, Int. J. Radiat. Oncol. Biol. Phys., 64, 419.
7. Liščák, R., Novotný, J., Urgošik, D., Vladyka, V. and Šimonová, G. 2000, Radiosurgery, 3, 205.
8. Ohtakara, K., Hayashi, S. and Hoshi, H. 2011, J. Radiat. Res., 52, 592.
9. Hellerbach, A., Luyken, K., Hoevels, M., Gierich, A., Rueß, D., Baus, W. W., Kocher, M., Ruge, M. I. and Treuer, H. 2017, Radiation Oncology, 12, 136.
10. Sheth, N. S., Sim, S., Cheng, J., Lustgarten, J., Estin, D., Olson, T., Weiss, M., Murphy, S., Chen, Y. and Yang, J. 2011, Int. J. Radiat. Oncol. Biol. Phys., 81, S867.
11. Ruschin, M., Lee, Y., Beachey, D., Yeboah, C., Wronski, M., Babic, S., Lochray, F., Nico, A., Khan, L., Soliman, H. and Sahgal, A. 2016, Technology in Cancer Research & Treatment, 15, 130.
12. Sung, K. and Choi, Y. E. 2018, PLoS One, 13, e0196664.
13. Wösle, M., Krause, L., Sreenivasa, S., Vordermark, D. and Ciernik, I. F. 2018, Strahlenther. Onkol., 194, 929.
14. Wagner, T. H., Bova, F. J., Friedman, W. A., Buatti, J. M., Bouchet, L. G. and Meeks, S. L. 2003, Int. J. Radiat. Oncol. Biol. Phys., 57, 1141.

- 
15. Akpati, H., Kim, C. S., Kim, B., Park, T. and Meek, A. 2008, *Journal of Applied Clinical Medical Physics*, 9, 99.
  16. Wösle, M. 2020, *Z. Med. Phys.*, 30, 70.
  17. Weiß, C. 2001, *Basiswissen Medizinische Statistik*, 2nd ed., Springer-Verlag GmbH, Berlin, Heidelberg, New York.
  18. Kocher, M., Wittig, A., Piroth, M. D., Treuer, H., Seegenschmiedt, H., Ruge, M., Grosu, A.-L. and Guckenberger, M. 2014, *Strahlenther. Onkol.*, 190, 521.
  19. Paddick, I. 2000, *J. Neurosurg. (Suppl. 3)*, 93, 219.
  20. Wilke, L., Andratschke, N., Blanck, O., Brunner, T. B., Combs, S. E., Grosu, A.-L., Moustakis, C., Schmitt, D., Baus, W. W. and Guckenberger, M. 2019, *Strahlenther. Onkol.*, 195, 193.
  21. Bronstein, I. N. and Semendjajew, K. A. 1987, *Taschenbuch der Mathematik*, 23rd ed., Verlag Harri Deutsch, Thun, Frankfurt (Main).